DOI 10.1007/s11141-023-10242-2
*Radiophysics and Quantum Electronics, Vol. 65, No. 8, January, 2023*
*(Russian Original Vol. 65, No. 8, August, 2022)*

# SYNTHESIS OF AN ULTRA-WIDEBAND PULSE BY A LOG-PERIODIC ANTENNA WITH CONTINUOUS EXCITATION BY HARMONIC OSCILLATIONS

**K. V. Muzalevsky** *

UDC 520.272.2

*We propose a method for synthesizing ultra-wideband pulses using a vector network analyzer and a wideband transceiving log-periodic antenna. The transfer characteristic of the antenna-feeder transmission line of the system is described by the model of a two-port network whose S-matrix elements are calibrated for at least two heights of the antenna above the reflecting surface (metal plate). The proposed method of calibrating the transfer characteristic of a log-periodic antenna allows one to minimize the amplitude- and phase-frequency distortions, which are introduced to the sensing pulse by the antenna. Employing the developed method, we experimentally demonstrate a possibility of synthesizing an ultra-wideband pulse with a duration of 0.46 ns at the level of half amplitude of the envelope (when the pulse contains several field oscillations) using a log-periodic antenna with a passband of 1.36 to 4.88 GHz (at the level −10 dB). This method is specially developed for creating miniature radar systems using portable vector network analyzers and log-periodic antennas for applications to remote sensing of an underlying surface by ultra-wideband pulses from small-size unmanned aerial vehicles.*

## 1. INTRODUCTION

Using ultra-wideband pulse signals along with the methods of georadar subsurface sensing and antenna aperture synthesis [1–3] is a promising new direction of radar sensing of the soil humidity [4, 5] and conductivity [6], soil-surface deformations (by radar-interferometry techniques [7]), thickness and density of the snow cover [8, 9], possible minefields [3, 10–12], and topsoil thickness [13] from the platforms of small-size unmanned aerial vehicles (UAVs).

Small-size UAVs mainly use Vivaldi antennas [8, 11, 14], combined Vivaldi horn antennas [1, 2, 5, 10], and log-periodic antennas (LPAs) [2, 15–17] as transmitting and receiving ultra-wideband megahertz antennas. As distinct from the Vivaldi antennas and combined Vivaldi horn antennas, which allow one to form an ultra-wideband pulse containing several field oscillations, the sensing pulse which is formed by a log-periodic antenna is a radio pulse with a decreasing (in time) frequency of aperiodic oscillations of the high-frequency filling [18–21]. Such a structure of the pulse is explained by the design features of the log-periodic antenna in the form of a two-wire transmission line with coupled symmetric dipoles which are connected to the line and resonate at various frequencies [22] (the high-frequency dipoles are excited earlier than the low-frequency ones). As a result, the phase center of the antenna is displaced and one may observe a time delay between high-frequency and low-frequency components of the pulse spectrum, which are radiated from a log-periodic antenna [19–22]. The radio pulses, which are formed by a log-periodic antenna, contain many periods of field oscillations [18–21] and are not optimal for the subsurface sensing of layered media [23, 24].

* rsdkm@ksc.krasn.ru

L. V. Kirenskii Institute of Physics of Siberian Branch of the Russian Academy of Sciences, Krasnoyarsk, Russia. Translated from Izvestiya Vysshikh Uchebnykh Zavedenii, Radiofizika, Vol. 65, No. 8, pp. 677–686, August 2022. Russian DOI: 10.52452/00213462_2022_65_08_677 Original article submitted April 11, 2022; accepted August 31, 2022.

 

At the same time, the developed new structures of the antennas, which are similar to a log-periodic antennas using the linear law of variation in the resonant frequencies of the neighbor dipoles, are modified in such a way that it is possible to synthesize an ultra-wideband pulse containing only a few field oscillations [19]. Additional delay circuits (delay lines) are also used to minimize the amplitude- and phase-frequency distortions, which are brought to the sensing pulse [20, 25]. The methods for calibrating the phase-frequency characteristic (PFC) of the antenna to compensate for the frequency dispersion of the location of the phase center of a log-periodic antenna in the frequency band from 400 to 1200 MHz are proposed in [26]. In this case, the nadir-looking monostatic radar method was used to measure the delay times of three pulses reflected from the metal screen and synthesized by a log-periodic antenna using bandpass filters in the frequency ranges 500–750 MHz, 750–1000 MHz, and 1000–1200 MHz when the antenna was located at a fixed height above the metal screen. The measured time delays of the reflected pulses were recalculated for the apparent heights of the antenna locations above the metal plate. The obtained values of the apparent heights were used to estimate the displacement of the location of the antenna phase center as a function of frequency [26].

As distinct from the existing approaches, this work offers an original method of using a log-periodic antenna for forming an ultra-wideband pulse containing several field oscillations with realization of the ideas developed in [27, 28]. In [27], an ultra-wideband antenna without a considerable PFC dispersion in the operating frequency band (400–3440 MHz) was used and neither the amplitude-frequency characteristic (AFC) nor the PFC were subject to correction. In [28], a nanosecond video pulse was synthesized using a sequence of four radio pulses at multiple frequencies whose amplitudes and the time delays were corrected to eliminate the nonuniformities of the AFC and the PFC of the transceiving antenna system having the form of wideband dipole antennas. The above analysis shows that the problem of the possibilities of forming the ultra-wideband pulses by a log-periodic antenna using the methods of calibrating the antenna-feeder transmission line of the system without introducing additional changes to the antenna design remains poorly studied.

## 2. MODEL AND METHOD OF TRANSCEIVING-ANTENNA CALIBRATION

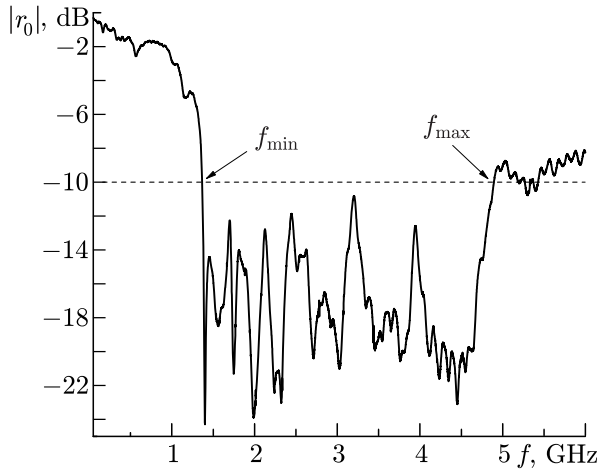


Fig. 1. Coefficient of reflection from a log-periodic antenna located in free space ($f_{\min} = 1.36$ GHz and $f_{\max} = 4.88$ GHz).

To calibrate the transfer characteristic of a transceiving log-periodic antenna [15], the monostatic scheme of radar sensing is realized. The maximum of the antenna pattern is oriented to nadir and the antenna is placed at a certain height $d_p$ above the ground surface ($p = 1, \ldots, N_{\text{h}}$, where $N_{\text{h}}$ is the number of antenna locations in the measurements). The height $d_p$ corresponds to the location of the antenna phase center, which is averaged in a certain frequency range of the antenna passband. The antenna-feeder line is represented as a two-part network [29, 30] whose $S$-matrix elements ensure relation between the complex amplitudes of the incident and reflected waves in the plane of input connection of the antenna. The vector network analyzer is used as a generating and recording unit. In this case, the coefficient $r(f, d_p)$ of reflection from the antenna, which is measured by the analyzer in the calibration plane (which coincides with the plane of the input connection of the antenna) can be written in the form [29, 30]

$$r(f, d_p) = r_0(f) + \frac{G(f, d_p)H(f)}{1 - S_{22}(f)G(f, d_p)}, \tag{1}$$

where $r_0(f)$ is the coefficient of reflection from the antenna if it is located in free space (see Fig. 1), $f$ is the electromagnetic-field frequency, $H(f)$ is the complex transfer function of the antenna, $S_{22}$ is the coefficient

of reflection of a wave (toward the directed radiation of the antenna) from the plane crossing the antenna phase center, and $G(f, d_p)$ is the transfer function of the sounded half-space with the point source located at the height $d_p$ above the air–medium plane interface. The transfer function $G(f, d_p)$ in model (1) can be written as follows:

$$G(f, d_p) = R(f)g(f, d_p), \qquad g(f, d_p) = \frac{1}{4\pi}\frac{\exp(4\pi i f d_p/c)}{2d_p}, \tag{2}$$

where $i$ is the imaginary unit, $g(f, d_p)$ is the three-dimensional scalar Green's function [31, 32], $R(f)$ is the Fresnel reflection coefficient of a plane wave which is normally incident on the air–soil interface, and $c$ is the light speed in free space.

As distinct from the antenna-calibration process [29, 30], the spherical divergence of the wave front of the radiated and received waves in the model described by Eqs. (1) and (2) is taken into account using the scalar Green's function $g(f, d_p)$. On the other hand, if the constants related to the amplitude of a point source are neglected, model (2) corresponds to the exact analytical expression for the Green's function of the horizontal electric dipole located at the height $d_p$ above the dielectric half-space, which was obtained in the far zone [20, 33] (the far-zone conditions are always satisfied for the UAV flight height). Such a simplification of an exact analytical expression of the Green's function allows one to propose an original (with respect to [29, 30]) method for calibrating the parameters of the model of Eqs. (1) and (2).

If a log-periodic antenna is located in free space ($G(f, d_p) = 0$ for $d_p \to \infty$), it is possible to measure the reflection coefficient $r_0(f)$. For brevity, we denote it as $r_0$. In this work, $r_0$ was measured on a large street area with the antenna located at a height of several meters above the ground with short grass so that the antenna-pattern maximum was oriented to the zenith. Then, measuring the reflection coefficients $r_1 = r(f, d_1)$ and $r_2 = r(f, d_2)$ for two arbitrary locations with the heights $d_1$ and $d_2$ of the antenna phase center above the metal screen, one can obtain the expression for the ratio of reduced reflection coefficients in the form

$$\Delta_{12} \equiv \frac{r_1 - r_0}{r_2 - r_0} = \frac{d_2}{d_1}\exp[4\pi f i\,(d_2 - d_1)/c]. \tag{3}$$

When deriving Eq. (3), we neglected the wave re-reflection between the antenna and the sounded half-space and assumed that $S_{22} \approx 0$ in Eq. (1). Equation (3) is independent of neither the transfer function $H(f)$, nor the reflection coefficient $R(f)$, which allows us to determine $d_1$ and $d_2$ from the solution of the system of nonlinear equations

$$d_2/d_1 = |\Delta_{12}|, \qquad d_2 - d_1 = \frac{c}{4\pi f}\arg\Delta_{12}, \tag{4}$$

where $|\Delta_{12}|$ and $\arg\Delta_{12}$ are the absolute value and the phase of the ratio of reduced reflection coefficients (3), respectively.

In this work, $d_2/d_1$ and $d_2 - d_1$ are estimated on the average for the entire operating frequency range of the log-periodic antenna. After finding the difference $d_2 - d_1$, the absolute (unwrapped) phase $c\arg\Delta_{12}/(4\pi)$ was calculated. The remaining unknown transfer function $H(f)$ is obtained from Eqs. (1) and (2) as

$$H(f) = \frac{H_1(f) + H_2(f)}{2}, \qquad H_1(f) = \frac{r_1 - r_0}{G(f, d_1)}, \qquad H_2(f) = \frac{r_2 - r_0}{G(f, d_2)} \tag{5}$$

if $R(f) \equiv -1$ in Eq. (2). To estimate the mean values and the confidence intervals of variations of the quantities $H(f)$ and $d_p$ in Eqs. (1) and (2), the reflection coefficient $r(f, d_p)$ was measured for a set of various antenna-location heights $d_p$ above the metal screen. Using the pairwise combination of the measured reflection coefficients $r_k$ and $r_j$ at the $k$th and $j$th heights, respectively, the obtained systems of Eqs. (3)–(5) can yield the mean values of the locations of the antenna-phase centers and the mean value of the complex transfer function $H(f)$.

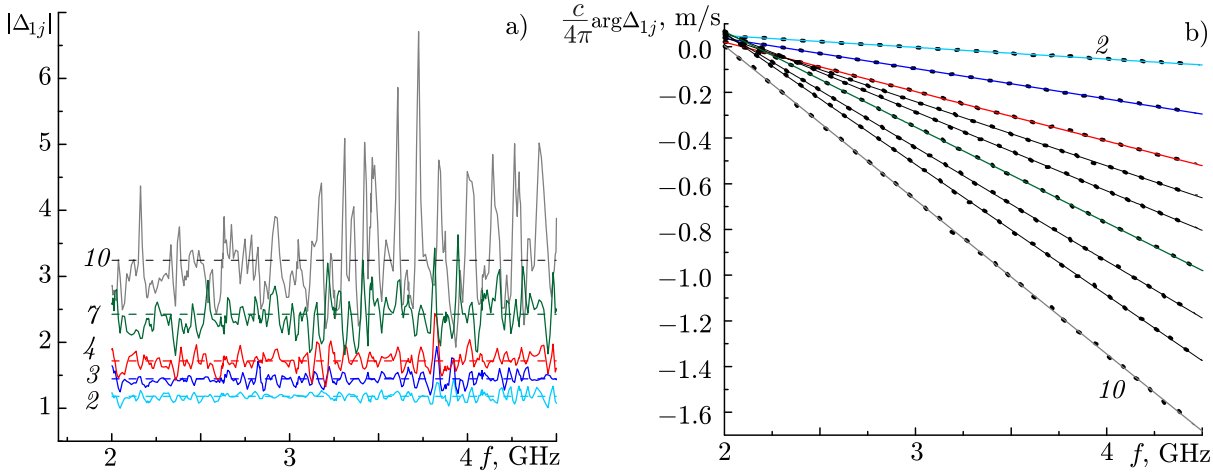


Fig. 2. The absolute value $|\Delta_{1j}|$ (*a*) and the absolute phase $c/(4\pi)\arg\Delta_{1j}$ (*b*) of the ratio of the reduced reflection coefficients measured at the heights $h_j$ ($h_2 = 0.31$ m, $h_3 = 0.391$ m, $h_4 = 0.475$ m, $h_5 = 0.54$ m, $h_6 = 0.604$ m, $h_7 = 0.678$ m, $h_8 = 0.757$ m, $h_9 = 0.83$ m, and $h_{10} = 0.932$ m) with respect to the height $h_1 = 0.26$ m. The solid and the dashed lines on panel *a* correspond to the measurements and the mean values, respectively, and the markers and the solid lines on panel *b* correspond to the measurements and the linear regression, respectively. The numbers of the curves correspond to the number of the height $h_j$

## 3. TRANSCEIVING ANTENNA CALIBRATION PROCEDURE

The coefficient of reflection from the antenna was measured in the frequency range from 1 to 5 GHz using a vector network analyzer "Agilent FieldFox 9927A," which was connected to the log-periodic antenna by an N-SMA coaxial junction and a 20 cm-long coaxial cable. Before the measurements, the analyzer was warmed up for 30 min and then it was calibrated using the mechanical set (complete two-port calibrator "Agilent 85518A" of the type-N50Ω). As an example, Fig. 2 shows the absolute value $|\Delta_{1j}|$ and the absolute (unwrapped) phase $c\arg\Delta_{1j}/(4\pi)$ of the ratio of reduced reflection coefficients, which were measured at the heights $d_2, \ldots, d_{10}$ with respect to the height $d_1$. The corresponding heights $h_j$ of the antenna location with respect to its lower edge were equal to 0.260, 0.310, 0.391, 0.475, 0.540, 0.604, 0.678, 0.757, 0.830, and 0.932 m for $j = 1, \ldots, 10$, respectively.

In accordance with the proposed method, the mean values of the locations of the antenna phase centers $d_k$ and $d_j$, where $k, j = 1, \ldots, 10$ (see Fig 3) were obtained for all possible combinations of nonrecurrent pairs ($k \neq j$) of the reflection coefficients $r_k$ and $r_j$, which were measured for the corresponding antenna-location heights $h_k$ and $h_j$. In the medium frequency range from 2.0 to 4.5 GHz, the phase center of the antenna is displaced from the front edge of the antenna (from the side of the directed radiation) over the distance $4.0 \pm 0.6$ cm to the antenna center (see Fig. 3). The corresponding value of $H_j(f)$ was obtained for each measured reflection coefficient $r_j$ on the basis of Eq. (5) using the obtained heights of the locations $d_j$ of the antenna phase centers. As a result, the magnitude $|\langle H(f)\rangle|$ of the mean value of the complex transfer function $H(f)$ of the antenna and the mean value $\langle\arg H(f)\rangle$ of the absolute phase of this function were estimated (see Fig. 4). At the boundaries of the antenna passband (1.36–4.88 GHz), the quantity of $|\langle H(f)\rangle|$ significantly decreases with increasing coefficient $|r_0(f)|$ of reflection from the antenna (and vice versa). In this case, the regions of the local minima of $|\langle H(f)\rangle|$ and the local maxima of $|r_0(f)|$ coincide. To equalize the AFC and the PFC of the transceiving log-periodic antenna when synthesizing the ultra-wideband pulses, the inverse-filtering method [28, 34], which ensured the maximum of the ratio of the signal to the root-mean-square value of noise, is used:

$$W_\alpha(f) = \frac{K_\alpha(f)}{\langle H(f)\rangle}, \tag{6}$$

where $K_\alpha(f)$ is the spectrum of the function of the Chebyshev window and $\alpha$ is the pulsation level (in dB)

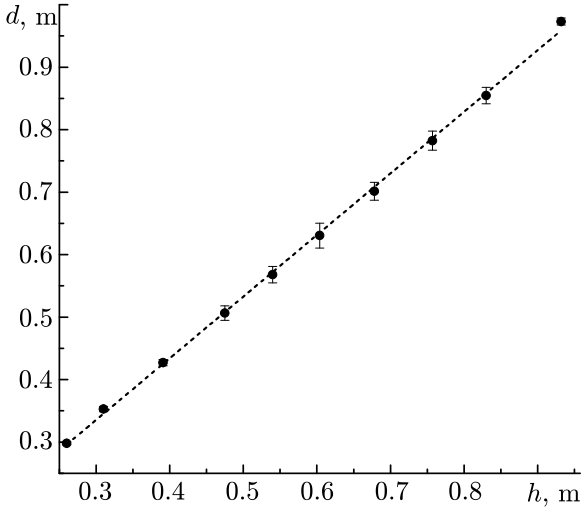


Fig. 3. The height $d$ of location of the antenna phase center above the metal plate as a function of the distances $h$ from the metal plate to the lower edge of the antenna. The markers correspond to the measured values of $d_p$ and the heights $h_p$, where $p = 1, \ldots, 10$ (the confidence intervals 95% are also shown) and the dotted line denotes the linear regression with the equation $d[\text{m}] = (0.040 \pm 0.006) + (0.986 \pm 0.010)h[\text{m}]$. The coefficient of determination of the linear regression is $R^2 = 0.999$ and the standard deviation is $\text{SD} = 6.9 \cdot 10^{-3}$ m

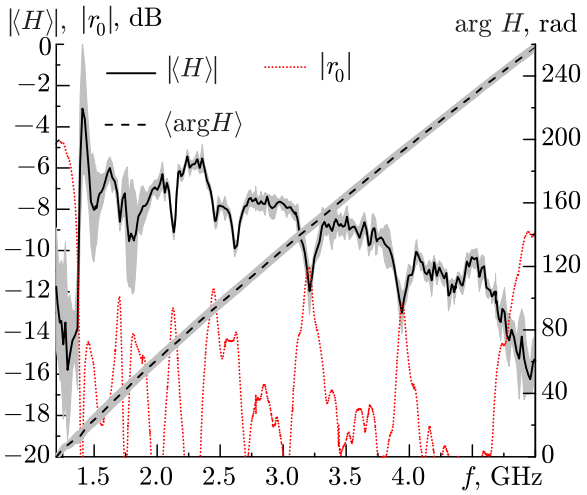


Fig. 4. The magnitude $|\langle H(f)\rangle|$ of the mean value of the complex transfer function of the transceiving antenna $|\langle H(f)\rangle|$ and the mean value $\langle \arg H(f)\rangle$ of the absolute phase of this function. The gray color is used to denote the confidence intervals (95%). The absolute value $|r_0(f)|$ of the coefficient of reflection from the antenna located in free space $|r_0(f)|$ is also shown.

beyond the passband of $K_\alpha(f)$. The function of the Chebyshev window [35] was used to ensure the minimum duration of the synthesized pulses (for the specified spectrum width) and decrease the noise level with respect to the main part of the pulse.

## 4. USING THE METHOD OF CALIBRATION OF A LOG-PERIODIC ANTENNA FOR SYNTHESIZING ULTRA-WIDEBAND PULSES. DISCUSSION OF EXPERIMENTAL RESULTS

The performed antenna calibration allows one to eliminate distortions, which are introduced by the antenna to the spectrum of the emitted and received ultra-wideband pulses, using the amplitude and the phase correction and the complex transfer function $\langle H(f)\rangle$. Employing the model de4scribed by Eqs. (1) and (2) and the Fourier transform, one can obtain an expression for calculating the signal $\dot{s}(t, d_p)$ of the ultra-wideband pulse, which is synthesized using a log-periodic antenna:

$$\dot{s}(t, d_p) = \int_{f_{\min}}^{f_{\max}} \exp(-2\pi i f t)[r(f, d_p) - r_0(f)]\, W_\alpha(f)\, \mathrm{d}f, \tag{7}$$

where $t$ is the time, and $f_{\min}$ and $f_{\max}$ are the minimum and maximum frequencies in the spectrum of the synthesized ultra-wideband pulse, respectively. Integral (7) was evaluated using the interpolation Gaussian quadrature [36]. In this case, the integration interval was splitted into 20 segments such that the Gaussian quadrature with 24 nodes was used on each segment [36]. This partitioning number ensured an absolute error of evaluating integral (7) in the time interval from 0 to 20 ns at a level not exceeding $10^{-2}$. Finally,

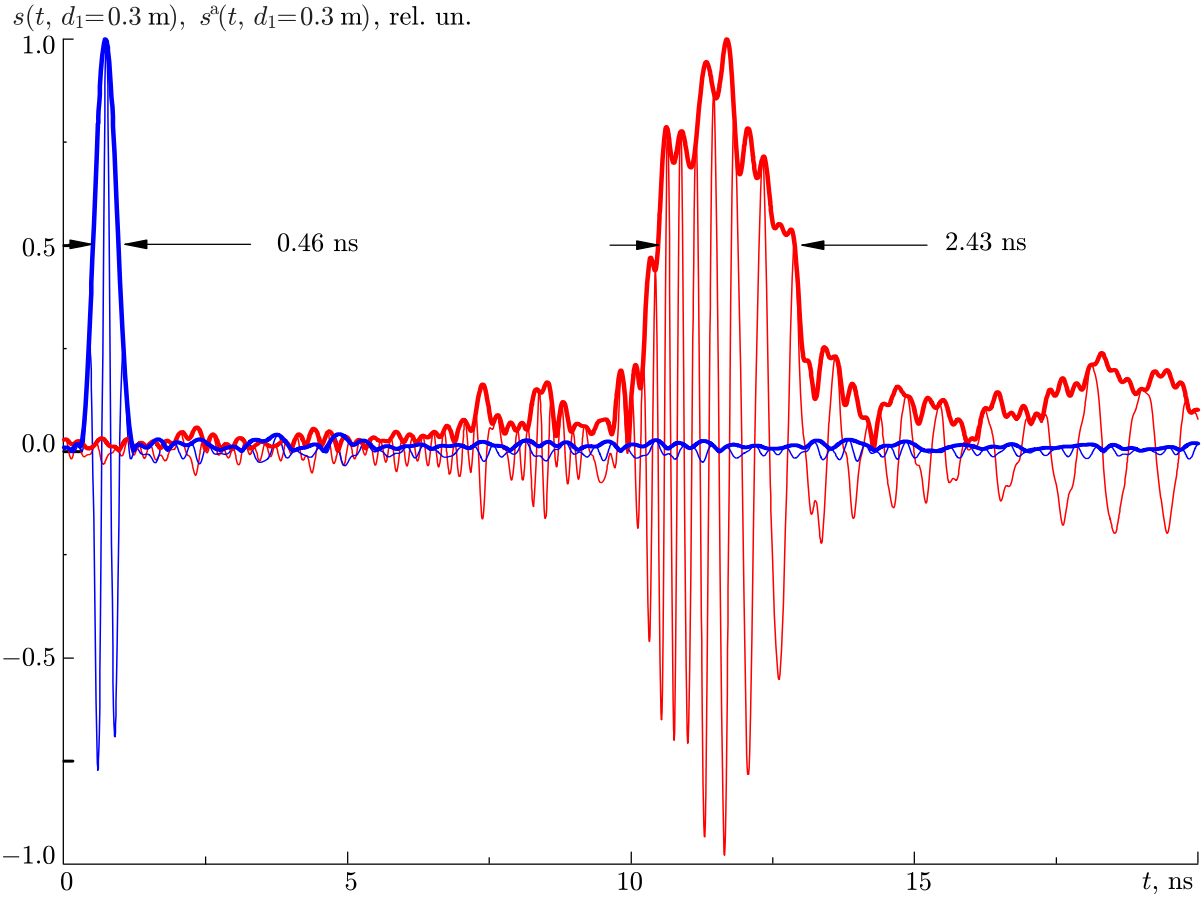


Fig. 5. The time waveforms (the thin lines) and the envelopes (the thick lines) of the sensing pulses before (red lines) and after (blue lines) the correction of the AFC and PFC of a log-periodic antenna. The waveforms are normalized to the maxima of the amplitudes of the envelopes of the corresponding pulses.

the time waveform $s(t, d_p)$ and the upper envelope $s^{\text{a}}(t, d_p)$ of the synthesized ultra-wideband pulse can be calculated as follows:

$$\dot{s}(t, d_p) = 2\text{Re}\, \dot{s}(t, d_p), \qquad s^{\text{a}}(t, d_p) = 2|\dot{s}(t, d_p)|. \tag{8}$$

Equations (7) and (8) realize the method of synthesis of the ultra-wideband pulses with correction of the AFC and the PFC of the antenna.

To test the above-proposed method of synthesizing ultra-wideband pulses, we measured the coefficient $r(f, d_p)$ of reflection from a layer of air-dried sand with a thickness of 23.5 cm, which was located on a metal plate in cases where the sand layer was covered or uncovered by the metal plate ($1.5 \times 1.5$ m). Sand with the volume humidity 1–2% and the density 1.46 g/cm$^3$ was placed in a square wooden box with sides of about 2 m. When sounding to nadir, the lower end of the antenna was located at various heights above the air–sand or air–metal screen interface.

As an example, Fig. 5 shows the time waveforms of the pulses $s(t, d_1 = 0.3\,\text{m})$ and $s^a(t, d_1 = 0.3\,\text{m})$, which are calculated on the basis of Eqs. (6)–(8) with and without correction ($W_\alpha(f) \equiv 1$) of the antenna AFC and PFC. When calculating the Chebyshev-window function $K_\alpha(\omega)$, the pulsation level outside the passband from $f_{\min} = 1.36$ GHz to $f_{\max} = 4.88$ GHz was $\alpha = -55$ dB. The duration of the synthesized ultra-wideband pulse using a log-periodic antenna and the developed method was 0.46 ns (for the level of half amplitude of the pulse envelope) for the noise level about $-40$ dB outside the main part of the pulse. Using the correction of the antenna AFC and PFC allows one to more than a factor of five reduce the duration of the synthesized ultra-wideband pulse compared with a radio pulse, which is formed without correction (see Fig. 5). The time waveforms of the envelopes of the ultra-wideband pulses synthesized on the basis of

the developed method, which are reflected from a sand layer and a sand layer covered by a metal plate, are shown in Fig. 6 (the antenna-location height is $d_4 = 0.515$ m). The arrival times of the ultra-wideband pulses, which are reflected from the air–metal screen interface (Fig. 6, curve *1*) and air–sand interface (Fig. 6, curve *2*) are almost equal to $2.95 \pm 0.01$ ns. The arrival time of the ultra-wideband pulse, which is reflected from the lower boundary of the sand layer (Fig. 6; curve *3*), equals 6.00 ns. The refractive-index value 1.82, which is calculated using the pulse-propagation time $\Delta t = 3.05$ ns inside the sand layer with its known thickness, turned out to be close to the sand refractive index 1.74 measured by the coaxial-waveguide method [37] at the center frequency of the sensing pulse. The good agreement of these estimates also confirms the efficiency of the proposed method of synthesis of ultra-wideband pulses.

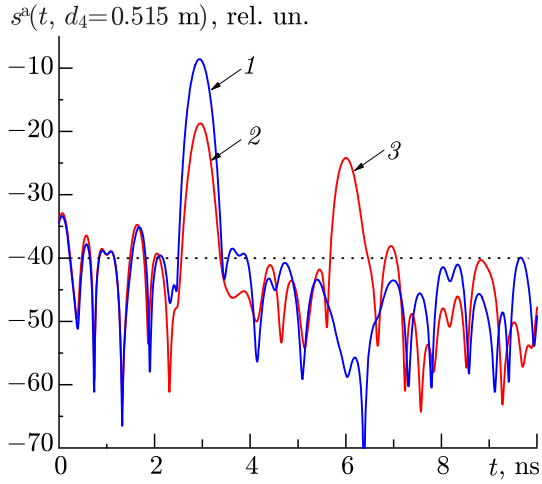

Fig . 6. The envelopes of the pulses reflected from a sand layer covered by a metal plate (*1*) and without a metal plate (*2* and *3*).

## 5. CONCLUSIONS

In this work, a method for synthesizing an ultra-wideband pulse with a duration of 0.46 ns (at the level of half amplitude of the envelope ), which contains one and a half periods of the field oscillation, has been developed using a vector circuit analyzer and a transceiving wideband log-periodic antenna with a passband from 1.36 to 4.88 GHz (at the level −10 dB). The proposed method for synthesizing ultra-wideband pulses does not require modifications in the log-periodic antenna design and can be realized in the form of an additional software calibration of the antenna-feeder transmission line. The method can be used for applications to remote sensing of the underlying surface by ultra-wideband pulses from small-size UAVs using portable vector network analyzers similar to those considered in [38].

This work was supported by the Russian Science Foundation and the Krasnoyarsk Regional Science Foundation (project No. 22–17–20042).

## REFERENCES

1. M. Schartel, R. Burr, W. Mayer, et al., in: *IEEE MTT-S Int. Conf. on Microwaves for Intellegent Mobility, 2018. April 15–17, 2018, Munich, Germany.* https://doi.org/10.1109/ICMIM.2018.8443503
2. M. Schartel, K. Prakasan, P. Hügler, et al., in: *IEEE Int. Geoscience and Remote Sensing Symposium, July 22–27, 2018, Valencia, Spain*, pp. 8420–8423. https://doi.org/10.1109/IGARSS.2018.8518905
3. M. García Fernández, Y. Álvarez-López, A. A. Arboleya, et al., *IEEE Access*, **6**, 45100–45112 (2018). https://doi.org/10.1109/ACCESS.2018.2863572
4. M. Moghaddam, S. Prager, A. Melebar, et al., in: *Earth Science Technology Forum, June 24, 2021.*, https://esto.nasa.gov/forums/estf2021/Presentations/June24/Moghaddam_GPR_ESTF2021.pdf
5. K. Wu, G. A. Rodriguez, M. Zajcet, et al., *Remote Sens. Environ.*, **235**, 111456 (2019). https://doi.org/10.1016/j.rse.2019.111456
6. K. Wu, E. Jacquemin, L. Palt, et al., in: *NSG2021 27th European Meeting on Environmental and Engineering Geophysics, August 29–Septemner 2, 2021*, https://doi.org/10.3997/2214-4609.202120117
7. D. Luebeck, C. Wimmer, L. F. Moreira, et al., *Remote Sens.*, **12**, No. 5, 778 (2020). https://doi.org/10.3390/rs12050778

8. R. O. R. Jenssen and S. K. Jacobsen, *Remote Sens.*, **13**, 2610 (2021). https://doi.org/10.3390/rs13132610
9. K. V. Muzalevsky, *Zh. Radioélektron*, No. 8, 1–16 (2021). https://doi.org/10.30898/1684-1719.2021.8.1
10. D. Šipoš and D. Gleich, *Sensors*, **20**, No. 8, 2234 (2020). https://doi.org/10.3390/s20082234
11. M. García Fernández, G. Álvarez-Narciandi, Y.Álvarez-López, et al., *ISPRS J. Photogramm. Remote Sens.*, **189**, 128–142 (2022). https://doi.org/10.1016/j.isprsjprs.2022.04.014
12. A. Heinzel, M. Schartel, R. Burr, et al., *Proc. SPIE*, **11003**, p. 1100304 (2019). https://doi.org/10.1117/12.2518587
13. J. Hou, Y. Yan, P. Cong, et al., *IOP Conf. Series: Earth and Environmental Science*, **719**, 042074 (2021). https://doi.org/10.1088/1755-1315/719/4/042074
14. M. García Fernández, Y. Álvarez-López, F. Las-Heras, et al., *Remote. Sens.*, **11**, No. 20, 2357 (2019). https://doi.org/10.3390/rs11202357
15. G. Ludeno, I. Catapano, A. Rengab, et al., *Remote Sens. Environ.*, **212**, 90–102 (2018). https://doi.org/10.1016/j.rse.2018.04.040
16. G. Fasano, I. Catapano, A. Rengab, et al., *Int. Conf. on Unmanned Aircraft Systems (ICUAS), June 13–16, 2017, Miami, USA*, pp. 1316–1323. https://doi.org/10.1109/ICUAS.2017.7991432
17. M. A. Yarlequé, S. Alvarez, H. J. Martínez, et al., in: *Int. Conf. on Electromagnetism in Advanced Applications, September 11–15, 2017, Verona, Italy*, pp. 1646–1648. https://doi.org/10.1109/ICEAA.2017.8065606
18. R. Burr, M. Schartel, P. Schmidt, et al., *IEEE MTT-S Int. Conf. on Microwaves for Intelligent Mobility, April 15–17, 2018, Munich, Germany*. https://doi.org/10.1109/ICMIM.2018.8443526
19. F. Merli, J.-F. Zurcher, A. Freni, and A. K. Skrivervik, *IEEE Trans. Antennas Propag.*, **57**, No. 11, 3458–3466 (2009). https://doi.org/10.1109/TAP.2009.2027140
20. A. Khaleghi, H. S. Farahani, and I. Balasingham, *IEEE Antennas Wireless Propag. Lett.*, **10**, 967–970 (2011). https://doi.org/10.1109/LAWP.2011.2167735
21. W. Sörgel and W. Wiesbeck, *EURASIP J. Appl. Sign. Process.*, **3**, 296–305 (2005). https://doi.org/10.1155/ASP.2005.296
22. A. L. Drabkin, V. L. Zuzenko, and A. G. Kislov, *Antenna Feeder Devices* [in Russian], Sovetskoe Radio, Moscow (1974).
23. M. I. Finkel'shtein, V. I. Karpukhin, V. A. Kutev, and V. N. Metelkin, *Subsurface Radar* [in Russian], Radio i Svyaz', Moscow (1994).
24. D. J. Daniels, *Ground Penetrating Radar,* The Institution of Electrical Engineers, London (2004).
25. P. Rulikowski and J. Barrett, *IEEE Microw. Wireless Comp. Lett.*, **18**, No. 5, 356–358 (2008). https://doi.org/10.1109/LMWC.2008.922131
26. M. García Fernández , Y. Álvarez-López, A. de Mitri, et al., *Remote Sens.*, **12**, No. 11, 1833 (2020). https://doi.org/10.3390/rs12111833
27. L. A. Robinson, W. B. Weir, L. Young, et al., *Proc. IEEE*, **62**, No. 1, 36–44 (1974). https://doi.org/10.1109/PROC.1974.9383
28. M. I. Finkel'shtein and V. A. Kutev, *Radiotekh. Élektron.*, **17**, No. 10, 2107–2112 (1972).
29. V. A. Mikhnev and P. Vainikainen, *IEEE Trans. Geosci. Remote Sens.*, **41**, No. 1, 75–80 (2003). https://doi.org/10.1109/TGRS.2002.808060
30. S. Lambot, E. C. Slob, I. van den Bosch, et al., *IEEE Trans. Geosci. Remote. Sens.*, **42**, No. 11, 2555–2568 (2004). https://doi.org/10.1109/TGRS.2004.834800

31. L. Tsang, J. A. Kong, and K.-H. Ding, *Scattering of Electromagnetic Waves: Theories and Applications. Vol. 1*, Wiley, Hoboken (2001).

32. G. T. Markov and A. F. Chaplin, *Excitation of Electromagnetic Waves* [in Russian], Radio i Svyaz', Moscow (1983).

33. C. Y. Kee and C. Wang, in: *IEEE Int. Symp. on Antennas and Propagation & USNC/URSI National Radio Science Meeting, July 9–14, 2017, San Diego, USA*, pp. 1357–358. https://doi.org/10.1109/APUSNCURSINRSM.2017.8072721

34. L. A. Vainshtein and V. D. Zubakov, *Isolation of Signals against a Background of Random Interference* [in Russian], Sovetskoe Radio, Moscow (1960).

35. F. J. Harris, *Proc. IEEE*, **66**, No. 1, 51–83 (1978). doi: 10.1109/PROC.1978.10837.

36. M. Abramowitz and I. A. Steagun, eds., *Handbook of Special Functions with Formulas, Graphs, and Tables*, Dover, New York (1972).

37. V. L. Mironov, I. P. Molostov, Y. I. Lukin, and A. Y. Karavaisky, in: *Int. Siberian Conf. on Control and Communications (SIBCON), September 12–13, 2013, Krasnoyarsk, Russia.* https://doi.org/10.1109/SIBCON.2013. 6693609

38. https://planarchel.ru/catalog/analizatory_tsepey_vektornye/vektornye_reflektometry_serii_caban/reflektometr-vektornyy-caban-r60/